RSC Applied Polymers

ROYAL SOCIETY OF CHEMISTRY

PAPER

View Article Online
View Journal | View Issue

Cite this: *RSC Appl. Polym.*, 2025, **3**, 1289

Impact of polymer molecular weight blends on the powder bed fusion process and the properties of polypropylene printed parts†

Akan George,[a] Jackson S. Bryant,[b] Timothy Taylor,[a] Michael J. Bortner,[b] Christopher B. Williams[b] and Mark D. Dadmun *[a]

Designing and controlling the molecular characteristics of polymeric feedstocks is crucial for creating robust structures *via* the powder bed fusion (PBF) process. To explore the impact of a powder's molecular weight on printed part structure and properties, thermally induced phase separation was employed to produce spherical, appropriately sized polypropylene (PP) powders formed from individual unimodal molecular weights and molecular weight blends. More precisely, these powders are composed of 12 000 Daltons PP (12k), 250 000 Daltons PP (250k), or 340 000 Daltons PP (340k), as well as their blends (50/50 wt% of 12k/250k, 12k/340k, 250k/340k, and 33/33/33 wt% of 12k/250k/340k). Analysis of the printed parts from these powders shows that the blended molecular weight (M_w) samples exhibit lower void space and higher crystallinity than the unimodal M_w counterparts. More importantly, dynamic mechanical analysis of the printed parts shows a substantial increase in storage modulus for blended molecular weight samples compared to unimodal M_w counterparts. This significant enhancement in the mechanical property of the blended molecular weight samples is due to improved coalescence dynamics driven by the powders' decreased melt viscosity. Improved coalescence reduces the void space in the printed parts, thereby improving mechanical performance. These results, therefore, provide a molecular-level understanding of the mechanism by which low M_w additives improve PBF processability, presenting avenues to augment the macroscopic properties of the printed parts. Additionally, the powder design approach presented in this work is cost-effective and offers a simple strategy to enhance the final part properties across various materials in additive manufacturing.

Received 26th February 2025,
Accepted 28th June 2025

DOI: 10.1039/d5lp00055f

rsc.li/rscapplpolym

1. Introduction

Powder bed fusion (PBF), also known as selective laser sintering (SLS), is an additive manufacturing (AM) process in which objects are created by using laser energy to melt and coalesce powders in a layer-by-layer fashion.[1,2] The PBF process offers numerous advantages among polymer AM technologies, including the ability to process semi crystalline polymers, high geometrical flexibility, and the ability to create customized parts without the need for dedicated support structures.[2,3] However, despite these advantages, parts produced through PBF often exhibit inferior mechanical properties when compared to those manufactured *via* traditional polymer processing techniques, such as injection molding.[3,4] At a molecular level, the poor mechanical properties associated with PBF fabricated parts are due to weak interfacial adhesion between layers. This weak interfacial adhesion is caused by poor chain mobility, the presence of void spaces that is the result of insufficient coalescence, and poor molecular chain entanglement at the interface between adjacent layers.[4–7] Moreover, the physics that govern the PBF process involves complex thermal histories that differ substantially from conventional manufacturing processes.

Another major constraint restricting the application of PBF for manufacturing is the limited range of materials available for the PBF process. For instance, the clear majority of the polymeric materials used in PBF are polyamides (PA12 and PA11).[8] In order to expand the availability of polymeric materials for PBF, it is important to understand the relationship between fundamental material properties of newly developed powders and their printability, as well as utilizing an economically viable method to make powders from a wide variety of polymers.

1.1. Impact of powder properties on PBF process

1.1.1. Effect of particle size and size distribution on PBF process. The first step in forming a layer in the PBF manufac-

[a]*The University of Tennessee, Knoxville, TN, USA. E-mail: Dad@utk.edu*
[b]*Virginia Polytechnic Institute and State University, Blacksburg, VA, USA*
† Electronic supplementary information (ESI) available. See DOI: https://doi.org/10.1039/d5lp00055f

turing process is powder recoating, which involves spreading polymer powder evenly onto the powder print bed using a roller.[1] Efficient flowability during this powder-spreading step is imperative to achieve a densely packed powder bed that leads to more dense printed parts.[1] The flowability of the powder during the recoating process depends on the powder size and shape; powders with a spherical shape and smooth surface are desirable in the PBF process because of their better flowability and packing efficiency.[1,9,10] If particles are too small, they may "evaporate off" when exposed to the high-energy beam, fogging the optics and heating elements and thus reducing the efficiency of the print process.[11] Furthermore, excessively small particles can adhere to the recoating roller due to electrostatic forces.[12] In fact, Averardi *et al.* highlighted that using particles smaller than 10 μm in PBF tends to result in agglomeration or aggregates due to strong cohesive forces, hampering powder flowability and layer density.[13] Hence, utilizing powders with appropriate particle size and distributions in the PBF process is crucial for optimal printability.[10,13,14] A commonly recommended average particle size for powder bed fusion is usually 40–100 μm.

After the powder recoating process, a laser heats the powder to selectively melt the powder to form melt pools at points in the layer to build the structure.[1,9,10] However, large variations in particle size can result in the complete melting of small particles and only partial melting of large particles, where incomplete melting of the larger particles results in incomplete coalescence of the powders and voids in the printed parts.[5,15] The time needed to conduct the heat from the laser throughout the particle strongly depends on the particle size of the powder. For example, the amount of laser energy required to raise the temperature of the powder particle correlates directly with the particle size. This relationship can be estimated using eqn (1) and (2).[14]

$$Q = mc_p\Delta T \quad (1)$$

In eqn (1), Q is the heat energy, m is the mass of the powder particle, c_p is the specific heat capacity of the particle, and ΔT is the temperature difference. Replacing the mass of the particle in eqn (1) by the particle density (ρ) times volume of the particle shows the dependence of the amount of heat required to raise the temperature of the powder particle (Q) on the particle radius. This substitution leads to eqn (2), which shows that Q varies with the particle radius cubed, r^3.

$$Q = \frac{4\pi r^3}{3}\rho c_p\Delta T \quad (2)$$

Moreover, the characteristic time for heat conduction from the laser-illuminated area to the surrounding region of the particle, t_c, varies with the particle radius as r^2, as shown in eqn (3), where α is the thermal diffusivity of the particle.[14]

$$t_c = \frac{4r^2}{\alpha} \quad (3)$$

Eqn (2) and (3) offer a quantitative understanding of how powder particle size can impact the PBF process, where, under the same experimental condition, larger particles require more laser energy to melt and coalesce at a slower rate than smaller particles.[5,11,14] Additionally, the conduction of heat through larger particles takes a longer time than in smaller particles.[14] The absorptivity of laser energy by the particle also diminishes with increasing particle size, which is attributable to a reduction in the surface area-to-volume ratio. Smaller particles provide a larger surface area to absorb more laser energy, leading to a faster melting and coalescence rate.[13] Hejmady *et al.* showed that increasing particle radius from 30 to 105 μm, results in the ratio of the laser spot size to particle size decreasing from 0.66 to 0.19. This leads to the conclusion that with a larger particle, a substantial portion of the particle may not efficiently absorb the laser energy, resulting in a pronounced temperature gradient within the particle, consequently decreasing the coalescence kinetics.[14]

1.1.2. Effect of particle shape on PBF process. In the PBF process, the geometry of powder particles affects their ability to flow during the recoating process to form a thin layer.[1,16–19] A freely flowing powder is also required to achieve a high packing density within the powder bed and to minimize interstitial voids between particles prior to coalescence to create dense parts.[1] The flow of particles during recoating is also significantly influenced by interparticle forces. Spherical particles, for instance, result in minimal contact between particles, reducing inter-particle friction. This characteristic improves particle flowability, enhancing the overall flow dynamics during the recoating process.[16]

The packing quality of the powder bed also has a substantial impact on the heat transfer characteristics and flow of the molten materials during the printing process. Studies indicate that higher packing density of the powder in the bed minimizes void spaces between particles, thereby enhancing the thermal interaction among particles during sintering.[13,20] Numerous studies have correlated the packing efficiency of the powder bed to particle shape. For example, Schiochet Nasato *et al.* and Haeri *et al.* investigated the dependency of the packing density of the powder bed on the particle aspect ratio.[17,18] Their findings show that as the particle aspect ratio increases, the packing density of the powder bed decreases. Deng *et al.* show that with increasing particle aspect ratio, the distribution of contact angle between the particles becomes wider, resulting in less packing of the particles and increased void spaces between the particles.[19] Given these findings, spherical and regularly shaped particles are preferred in the PBF process due to their superior flowability characteristics and higher packing efficiency compared to non-spherical and irregularly shaped particles.

1.1.3. Effect of polymer molecular weight and viscosity on PBF process. After selective heating of the powder by the laser beam, the melted powders coalesce and then solidify upon cooling to form intra- and inter-layer bonds.[1,10] Polymer viscous flow and particle coalescence control densification and impact the final mechanical properties of the printed parts. Sufficient particle coalescence within one layer and across layers is essential to achieving a homogeneous structure with few defects and mechanically robust 3D-printed parts.[9]

Viscous flow is a crucial driving force of the coalescence phenomena in the PBF process.[10] Theoretical models, such as the Frenkel model describe viscous coalescence with critical parameters that govern the coalescence kinetics, including, polymer zero-shear viscosity and surface tension.[1,9,10,14] The polymer zero-shear viscosity is the viscosity of the material as the shear rate approaches zero. This is a limiting value that approximates the viscosity of the material when there is no shear applied to the sample. No mechanical pressure is applied to the polymer during the PBF process as opposed to the injection molding process;[21] thus the zero-shear viscosity is the appropriate parameter to model this process. This is quantitatively shown in the Frenkel model (eqn (4)), where an increase in the zero-shear viscosity leads to a decrease in the time evolution of the coalescence $\left(\frac{x}{a}(t)\right)$.[1]

$$\frac{x}{a}(t) = \left(\frac{3\Gamma t}{2a\eta_0}\right)^{\frac{1}{2}} \quad (4)$$

In eqn (4), x is the neck radius between two adjacent coalescing particles, a is the initial particle radius, t is the coalescence time, Γ is the surface tension of the polymer, and η_0 is the zero-shear viscosity of the polymer. η_0 is related to polymer molecular weight (M_w) *via* eqn (5), where c is a constant.[22]

$$\eta_0 = cM_w^{3.4} \quad (5)$$

The timescale associated with particle coalescence in the PBF process is only approximately 10 seconds;[10] thus, polymers with higher molecular weights, and higher viscosities, may not be exposed to the laser power long enough to melt and sufficiently flow to complete consolidation within this short timescale. Therefore, we hypothesize that designing polymeric materials with tunable zero-shear viscosity to improve polymer flow during coalescence could improve interfacial adhesion, powder consolidation, and thus part robustness.

1.2. Strategies to enhance consolidation of particles and improve mechanical strength in PBF printed parts

1.2.1. Manipulation of print settings. Various mechanistic approaches have been attempted to promote the consolidation of particles and improve mechanical strength in PBF printed parts. For instance, the effect of laser power on the density and the tensile strength of PA12 printed parts by PBF has been investigated by Yan *et al.*[23] Their findings show that the density and the tensile strength increase with increasing laser power until they reach a maximum value and then further increasing laser power results in the decrease in the density and the tensile strength. Similar results have been reported by Zhu *et al.* in the PBF of Polypropylene (PP).[24] The correlation between increasing laser power (P_L) and the improved mechanical properties of the PBF printed parts is not surprising, as it stems from the direct relationship demonstrated in eqn (6), where increasing P_L will consequently increase the energy the laser beam delivers to the polymer powder per unit area (the energy density [E_D]), assuming all other parameters remain constant.[1]

$$E_D = \frac{P_L}{D_l H_s V_S} \quad (6)$$

In eqn (6), H_s is the hatch spacing, D_l is the laser diameter, and V_S is the laser beam speed. Increasing laser power, thus, increases energy density, raising the powder temperature, which lowers the viscosity of the polymer, and fosters a faster coalescence during the printing process. However, increasing the energy density can lead to material degradation and dimensional errors in the printed structure.[23,24]

1.2.2. Material modification. Material degradation poses a significant limitation to parameter-based approaches to improving printed part properties. Therefore, material design, such as modifying the polymeric material rather than altering the physical print parameters and understanding how polymer feedstock molecular characteristics impact particle consolidation during printing are viable ways to design materials to fabricate mechanically robust 3D-printed parts. Hence, this study focuses on modifying the molecular characteristics of the polymer feedstocks to optimize the crucial consolidation processes in PBF.

In previous work by our group, designing bimodal molecular weight materials has been proven to enhance the mechanical performance of material extrusion-based 3D-printed structures. For example, Levenhagen *et al.* designed bimodal blend polylactic acid (PLA) filaments by incorporating lower molecular weight PLA additives into commercially available higher molecular weight PLA filament. The lower molecular weight PLA additives improve polymer chain diffusion between layers, strengthening the interfacial adhesion between layers in structures created by the fused filament fabrication (FFF) process, and result in mechanically robust 3D-printed parts.[25] Lower molecular weight additives in a polymer melt readily sequester to the interface of the filament, where they can more quickly form entanglement between layers relative to the diffusive processes of their higher molecular weight counterparts.[25,26]

Given this fundamental process and the importance of polymer molecular motion in particle coalescence in the PBF process, we hypothesize that such a molecular modification protocol will also improve the mechanical performance of polymer parts fabricated by PBF. From the Frenkel model, it is clear that the zero-shear viscosity is a dominant parameter that governs polymer flow during coalescence, and thus the coalescence process. Moreover, the zero-shear viscosity has a well-known relationship to polymer molecular weight (eqn (5)), opening avenues to control this crucial parameter by modifying the average molecular weight of the polymer. Thus, this work is designed to examine the impact of molecular weight blends of polypropylene (PP) powders on the PBF process and the properties of the printed parts.

To achieve this aim, we utilize thermally-induced phase separation (TIPS)[27,28] to create powders with bespoke molecular weight (M_w) distributions, where high molecular weight PP is blended with an identical, but low M_w, PP to form molecular weight blends of PP. By combining low molecular weight

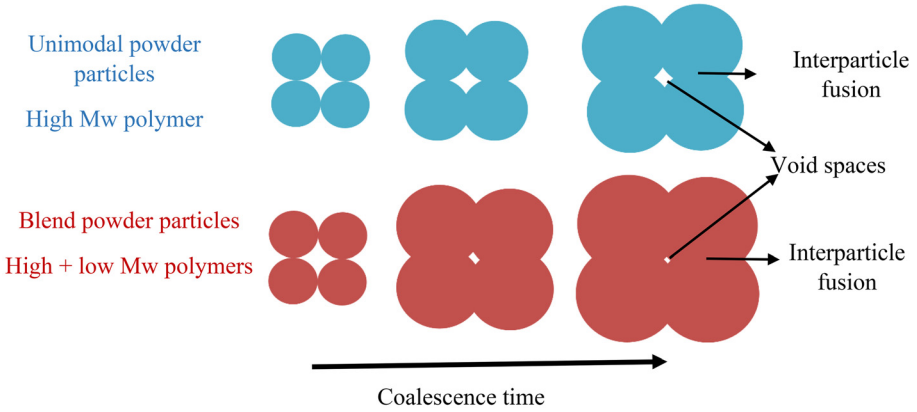

Fig. 1 Proposed strategy to enhance coalescence and decrease void space in high M_w polymer by molecular modification. Under the same experimental condition, molecular blend sample should exhibit higher level of coalescence and lower void space than unblended samples.

PP with high molecular weight PP, we expect the viscosity of the blend to be significantly lower than that of the high molecular weight PP, potentially facilitating molecular mobility and improving the coalescence dynamics during the PBF process. This targeted improvement of the coalescence process is shown schematically in Fig. 1. Thus, under the same thermal energy of the PBF process, we expect that the coalescence of the molecular weight blend powders will be faster, potentially reducing internal voids and creating a more robust structure relative to structures formed from neat high molecular weight polymer. As illustrated in Fig. 1, a high degree of coalescence and substantial void space reduction should result in improved densification and enhanced mechanical performance of the printed parts. Providing this understanding of molecular-level mechanisms governing particle fusion establishes a solid foundation for the strategic creation of polymeric feedstocks for improved PBF printing. Moreover, developing materials with molecular weight blends presents a cost-effective approach to tailor feedstocks, effectively tackling some of the existing challenges encountered in the PBF process. This work aims to provide a fundamental understanding of the mechanism by which polymer molecular weight and, thus zero-shear viscosity, controls the fabrication of structures in the PBF process. PP is an important thermoplastic as it is widely applicable across various industries due to its good mechanical performance, chemical stability, and relatively low cost.[24] Understanding how polymer molecular weight affects PBF fabrication will not only contribute to improving PP printability but also potentially pave the way for advancements in other materials processed by PBF.

2. Experimental methods

2.1. Materials

Isotactic polypropylene pellets with molecular weights of 12 000, 250 000, and 340 000 Dalton were purchased from Sigma-Aldrich. Xylene, ethanol, and silicone oil were purchased from Fisher Scientific. All chemicals were used without further purification. Throughout this work, molecular weights of 12 000, 250 000, and 340 000 Daltons will be denoted by 12k, 250k, and 340k Daltons, respectively.

2.2. Production of PP powders *via* thermally-induced phase separation (TIPS)

Thermally-induced phase separation (TIPS)[27,28] was used to form PP powders for PBF. With this process, PP powders were formed from neat 12k, 250k, and 340k PP pellets, 50/50 wt% blends of 12k/250k, 12k/340k, and 250k/340k and a 33/33/33 wt% blend of 12k/250k/340k. To fabricate each PP powder sample, 9 g of PP pellets were added into a 250 ml round bottom flask. 91 g of xylene was added, and the mixture was heated with a hotplate to 190 °C, stirred at 200 rpm, and refluxed for 1 hour to form a homogeneous solution. After 1 hour of reflux, the mixture was placed into a cold trap at 40 °C without stirring using a Fischer Isotemp containing a mixture of 50% water and 50% ethylene glycol as the refrigerant and quenched for 1 hour to precipitate the powders. After the quenching process, vacuum filtration separated the precipitate, where the PP powders were washed with ethanol three times to remove residual xylene. The obtained powders were then placed in a vacuum oven at 40 °C and dried until a constant mass is reached. The yield of the powder based on the initial pellet loading is 95–98%. The schematic representation for the PP powder formation is shown in Fig. S1.†

2.3. Characterization of the prepared PP powder

2.3.1. Evaluation of particle size distribution *via* laser diffraction particle size analyzer. The particle size and particle size distribution of the produced PP powders were determined with a Mastersizer 3000 laser diffraction particle size analyzer (Malvern Instruments Ltd). This analysis provides the particle size distribution and median diameter, D50, for all the prepared PP powders, where D50 represents the particle diameter value at 50% in the cumulative distribution. For each sample formulation, this experiment was repeated at least three times.

2.3.2. Scanning electron microscopy (SEM). Scanning electron microscopy (SEM) was performed to monitor the shape of the prepared powders. To obtain SEM micrographs of the samples, each sample was coated with a thin layer of gold to eliminate surface charging. The SEM used in this study is a ZEISS-EVO with high electron tension set at 20.00 kV.

2.3.3. Zero-shear viscosity. The zero-shear viscosities of the PP powders formed from TIPS were determined *via* rotational rheometry using an AR200ex rheometer from TA Instruments at Oak Ridge National Laboratory. The viscosity measurement was performed at 164 °C and at 0.005 s^{-1} shear rate. Disc-shaped specimens that were 25 mm diameter and 1 mm thickness were prepared by compression molding at 170 °C for 5 minutes under 2 metric tons load. A 25 mm diameter parallel plate was used. Before each rheological measurement, the sample was thermally stabilized for 10 minutes to ensure thermal equilibrium. The temperature was stabilized within 0.2 K for all measurements.

2.3.4 Molecular weight determination. The molecular weight and dispersity of the PP MW blend powder samples prepared *via* TIPS were determined by a high-temperature Size Exclusion Chromatograph (SEC), a Malvern high-temperature OMNISEC system, using 1,2,4 trichlorobenzene as the eluent, with solution concentrations ranging from 1.0 to 3 mg ml^{-1} and calibrated to polypropylene standards. Viscometer, refractive index, low-angle light scattering, and right-angle light scattering detectors were used to obtain the molecular weight and dispersity data.

2.3.5. Thermal analysis of PP powders. Data from differential scanning calorimetry (DSC) is used to establish the feasible PBF processing temperatures of the PP powders. The DSC data were obtained with a TA Instruments DSC Q2000. Approximately 5–10 mg of each sample was placed in standard aluminum pans with covers and the DSC curves were measured at a heating rate of 10 °C min^{-1} from 40 °C to 200 °C, followed by cooling to 40 °C at 10 °C min^{-1} under nitrogen purge gas flow. The PBF processing temperature ranges are defined as occurring between the onset melting temperature and the onset crystallization temperature.

The thermal stabilities of the PP powders were determined *via* thermogravimetric analysis (TGA) using a TA Instruments TGA Q50. Approximately 10 mg of each sample was heated from 40 °C to 600 °C at the rate of 10 °C min^{-1} under nitrogen gas. The thermal stabilities of the PP powders are obtained from the peak degradation temperature of the TGA curve.

2.4. Powder bed fusion of the prepared PP powders

All prepared powders were printed using a Prodways Promaker P2000 HT printer, which is equipped with a 60 W CO_2 laser. Using the processing temperature identified from DSC data, and based on preliminary experimental trials, samples were printed with a layer thickness of 100 μm as well as bed and feed temperatures set to 140 °C, a laser power of 50 W, beam velocity of 3750 mm s^{-1}, and hatch spacing of 0.3 mm. These print parameters correspond to an energy density (E_D) of 0.044 J mm^{-2}. Laser parameters were held constant for all powder specimens to enable direct evaluation of the impact of molecular weight on the structure and properties of the printed parts. The bed and feed temperatures were set conservatively to reduce the risk of powders prematurely melting and coalescing in the powder bed prior to energy deposition, which is more likely as these set temperatures approach the onset of melting for a powder. Tensile testing dogbones and rectangular prismatic structures (21 mm × 6 mm × 1 mm) for dynamic mechanical analysis (DMA) were printed from the fabricated PP powders, as shown in Fig. 2.

2.5. Characterization of the PP printed parts

2.5.1. Dynamic mechanical analysis (DMA). DMA (TA Instruments DMA Q800) was used to characterize the viscoelastic behavior of the printed samples. Storage and loss moduli curves were obtained with a frequency of 1 Hz and a strain of 0.1% where the temperature was ramped from −50 °C to 120 °C at 3 °C min^{-1}. Additionally, the glass transition temperature (T_g) of each printed sample was determined from the peak of the damping factor, tan δ. The DMA was performed in tensile mode. Two DMA runs were performed for two sample formulations to assess reproducibility, as shown in Fig. S5.† For the remaining material formulations, additional runs could not be completed due to limited sample availability and sample breakage during handling.

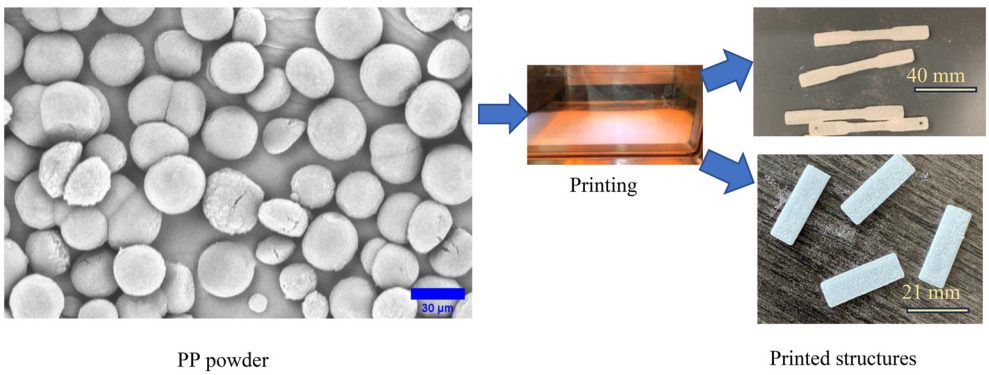

Fig. 2 Powder bed fusion of the PP powder. The tensile bars are formed from the 250K powder, while the rectangular DMA bars are formed from the 250K and 12K blend powder.

2.5.2. Evaluation of crystallinity and crystal structure of the PP printed parts. Differential scanning calorimetry (DSC) curves were analyzed to determine the crystallinity of the printed structures. DSC curves were obtained with a TA Instruments DSC Q2000 Approximately 5–10 mg of the printed samples were placed in standard covered aluminum pans and measured at a heating rate of 10 °C min^{-1} from 40 °C to 200 °C, followed by cooling to 40 °C at 10 °C min^{-1} under nitrogen purge gas flow. The percent crystallinity, X_C, of the polymer samples was calculated from the experimentally determined heat of fusion according to eqn (7).[24]

$$X_c = \frac{\Delta H_m}{\Delta H_m^\circ} \times 100\% \quad (7)$$

In eqn (7), ΔH_m is the measured melting enthalpy, of the printed structure, and ΔH_m° is the melting enthalpy of fully-crystalline PP material (209 J g^{-1}).[29] Wide-angle X-ray scattering (WAXS) was also performed to investigate the variation in crystalline structure among printed samples. WAXS curves were obtained using a Xenocs Xeuss 3.0 X-ray scattering instrument with a PILATUS3 R detector and an X-ray wavelength of 1.54 Å. The sample detector distance was 0.045 m. The printed solid samples were placed in a beam and scattered directly. All scans were obtained under a vacuum. Collected scans were analyzed using a Gaussian curve to obtain peak positions.

2.5.3. Void space evaluation *via* SEM and ImageJ software. Scanning electron microscopy (SEM) was used to determine the percent void space in the printed samples. Sample preparation included fracturing the PP printed samples with liquid nitrogen, followed by coating with a thin gold layer the sample surface to eliminate surface charging. The SEM used in this study is a ZEISS-EVO with high electron tension set at 5.00 kV, where an example image is shown in Fig. 3. To determine the percent voids, ImageJ was first used to convert the SEM images to black and white, eqn (8) was then used to determine percent voids in the sample. For each sample formulation, this experiment was repeated at least three times.

$$\text{Void space } \% = \frac{\text{total number of black pixels}}{\text{total number of black + white pixels}} \times 100. \quad (8)$$

3. Results and discussion

3.1. Particle size and distribution of fabricated PP powders

It is well known that the size of powder particles plays a critical role in governing particle flow dynamics during the recoating process, and thus directly affects the quality of the prepared powder bed and its packing density. Thus, employing the proper particle size and distribution is vital for effective absorption of laser energy and ensuring proper coalescence during the printing process. Forming polymer powder with proper size and distribution for the PBF process is challenging but is required to create molecularly designed powders that are suitable for use in polymer powder bed fusion. Our previous studies have demonstrated that the TIPS process provides pathways to fabricate polypropylene powders of targeted size and distribution that are suitable for PBF.[27,28] Fig. 4 shows the size distribution of the powders created for this study, for both the neat polymers and all of the molecular weight blends. This figure shows similar size distributions and the production of powders with average particle size, D50, that is consistent with the particle size range that is suitable for PBF. Table S1† presents the D50, D10, and D90 values for the PP particles formed *via* the TIPS process. The successful production of the PP powders with target average sizes across various molecular weight and blends underscores the significance and the ability of the TIPS process in this study to develop and rationally control the powder production method to create bespoke feedstocks to address current challenges in the PBF process. Moreover, producing these PP powders with uniform sizes for all samples allows researchers to eliminate the impact of particle size on the PBF process. Summarily, PP particles of similar size require similar energy absorption and the influence of particle size on flowability and coalescence are comparable, allowing for a more detailed examination of molecular weight effects on the PP molecular weight on the PBF fabrication process.

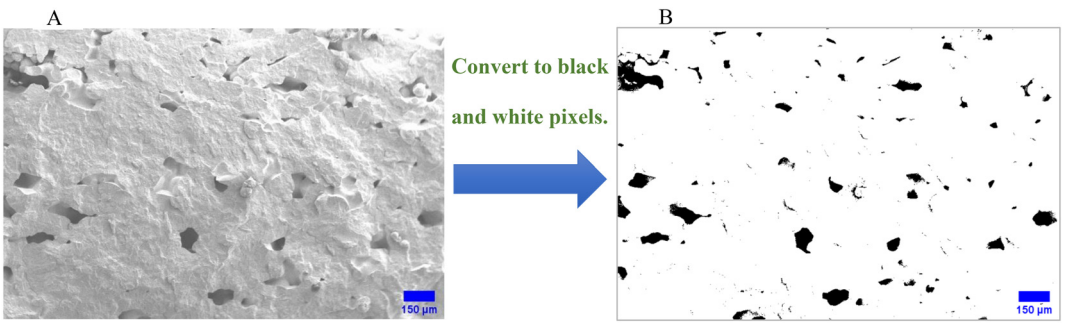

Fig. 3 Evaluation of void space in the printed sample *via* SEM and ImageJ. (A) SEM image of the printed sample showing the void spaces. (B) Converted SEM image of the printed sample to black and white pixels using ImageJ. Scale bar is 150 μm.

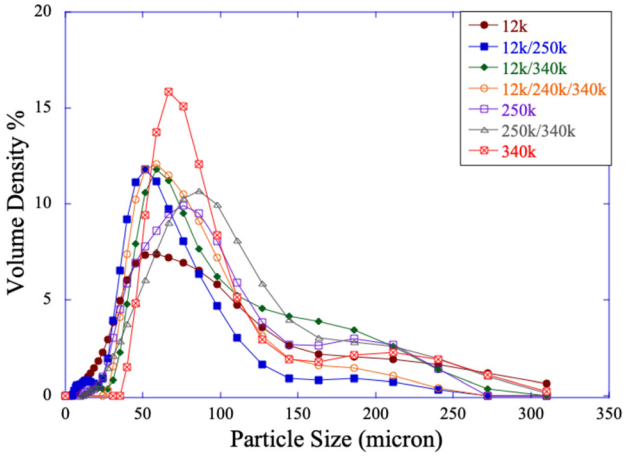

Fig. 4 Particle size and distributions of produced PP powders analyzed using laser diffraction. The average particle size, D50, is the proper size (58 μm–86 μm) for PBF.

3.2. SEM images of the structure of fabricated PP particles

Fig. 5 shows SEM images of the fabricated PP powders, where the particles are spherical with smooth surfaces. However, a closer examination of the SEM images shows that the powders formed from the neat 12k sample have some particles that are crumpled, while the powders formed from the neat 340k sample shows some particles that have rough surfaces. Intriguingly, these structural characteristics of the powder are eliminated when the 12k PP is blended with high molecular weight PP using the TIPS process. This structural transformation becomes apparent in the 12k/250k, 12k/340k, and 12k/250k/340k powder particles. These variations in structure could be attributed to the complex interactions occurring during the formation of droplets from blends in the TIPS process. The fact that all the PP samples have identical shapes implies similar particle aspect ratios, suggesting comparable configurations in the print bed during powder spreading. This structural similarity provides a foundation to eliminate the impact of particle shape on the PBF process in this study. This, in turn, allows for a focused investigation of how the molecular weight of the powders influences the PBF process and the properties of the resulting printed structures, as detailed below.

3.3. Tuning powder zero-shear viscosity

Coalescence is a fundamental aspect of the PBF process that directly impacts the strength, quality, and properties of printed parts. It depends intimately on the surface tension and zero-shear viscosity of the polymer. Table 1 shows the average molecular weights (M_w = weight average molecular weight, M_n = number average molecular weight) and the dispersity (M_w/M_n) of the PP powders made from the pure PP and their blends. It is evident that the inclusion of a polymer with lower chain length, 12k PP, notably modifies the average molecular weight and polydispersity of the 250k and 340k PP counterparts. Fig. 6 correlates the zero-shear viscosities at 164 °C of the powders to the weight average molecular weight of the polymers, M_w, showing reasonable agreement of the expected molecular weight dependence of the polymer viscosity (eqn (5)). The slight deviation of the molecular weight dependence of the polymer viscosity from eqn (5) is not uncommon. In particular, the zero-shear viscosity depends not only on the weight average molecular weight of the polymer but also on the polymer dispersity,[30,31] which also varies significantly in these samples.

More importantly, the introduction of 12k PP to higher molecular weight PP provides a controllable method to significantly alter the molecular level characteristics of the higher molecular weight polymers, substantially reducing their zero-shear viscosities; for instance, from 3027 Pa s for 250k to 349 Pa s for 12k/250k, and from 7031 for 340k to 426 Pa s for 12k/340k. The results of these studies, therefore, offer a pathway to understanding the mechanism by which the 12k PP additive impacts both the consolidation process of high molecular weight polymers and the overall quality of the printed structures. Moreover, the authors' prior examination of the particle coalescence of these exact powders shows that the addition of 12k significantly increases the coalescence rate of the powder.[32] The substantial decrease in zero-shear viscosity resulting from the addition of 12k PP is the dominant factor in the previously observed pronounced enhancement in coalescence.[32]

3.4. Impact of molecular weight on PP printability

All powders except that which is formed from the 12k PP were printable at the set processing parameters (section 2.4). These printed samples showed minimal warpage during printing, which led to printed samples that could be tested mechanically. The PBF printing of the 12k powder, however, showed unique behavior. As shown in Fig. 7, the structure that emerges from single layer scans did not match their defined geometry, which was a solid square in this case. While the outlines of the scanned layer can be seen, it was observed that the molten polymer shrank from its defined shape after scanning to form a ribbed structure. In this ribbed structure, many pathways are thicker than the layer height.

Coalescence of a molten polymer in PBF depends on both the zero-shear viscosity and surface tension of the polymer. It is hypothesized that for the 12k sample, the viscosity is so low, that the surface tension dominates the coalescence process, leading to a sample that "over-coalesces". Since PBF research is primarily conducted on engineering or high-performance polymers with molecular weight significantly greater than 12k, it is likely that this material is below a threshold viscosity necessary for proper coalescence whereas the majority of materials researched in literature are above this threshold. Due to the over-coalescence that occurred in the 12k sample after scanning, multi-layer samples were not printable. This observation also emphasizes the need to more thoroughly understand the impact of polymer molecular weight, viscosity, and melt surface tension on the printing process.

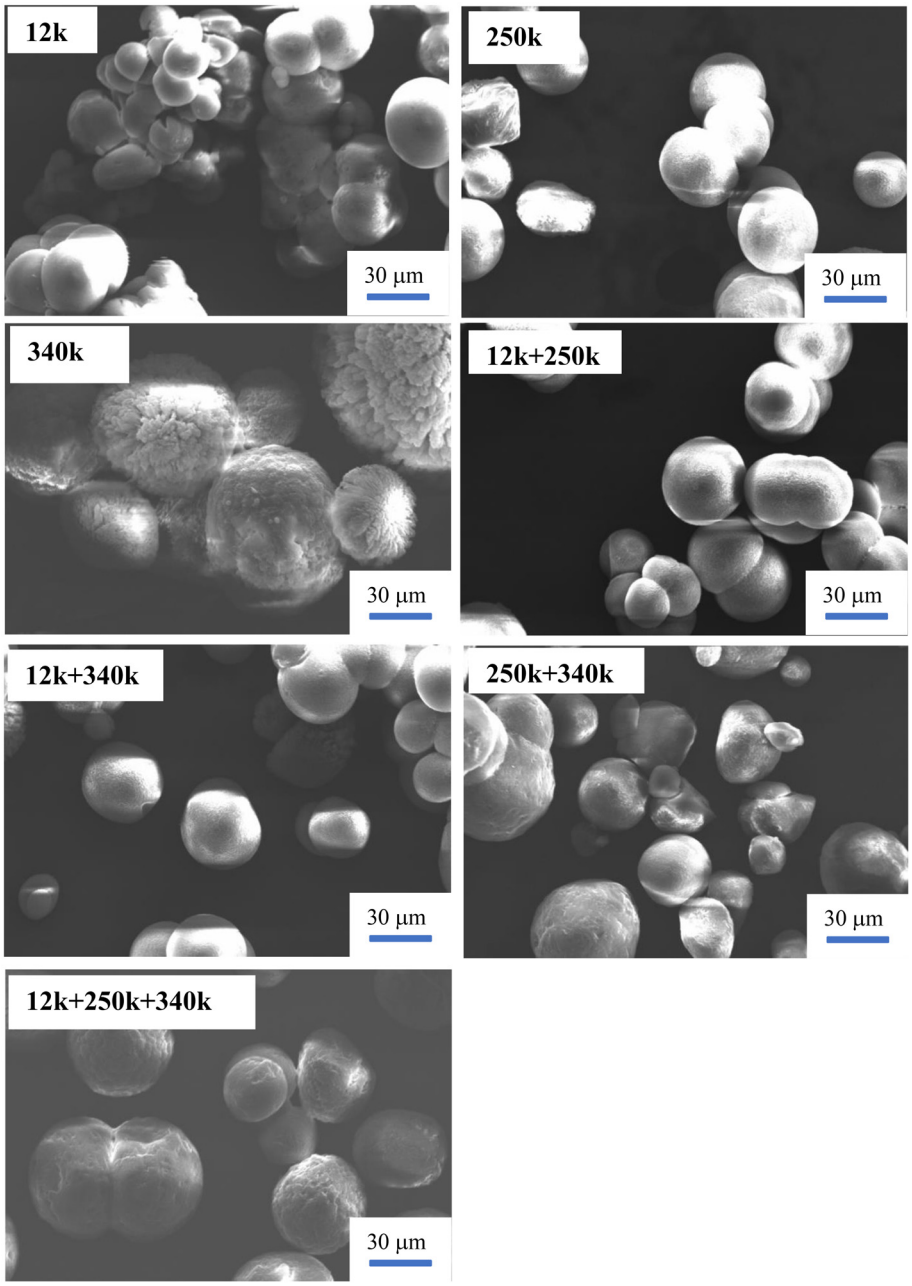

Fig. 5 Structures of PP powders obtained *via* scanning electron microscope. PP samples produced in this work are highly spherical. Scale bars are 30 microns.

The pictures of the printed structures with varying material formulations are shown in Fig. S2.† As illustrated in Fig. S2,† the samples exhibit a consistent appearance, suggesting that the material formulations do not have significant effect on the external characteristics of the fabricated parts.

3.5. Properties of the printed parts

The dynamic mechanical properties, tensile properties, and densities of the printed parts were measured. The results of the tensile properties and density studies (Fig. S3 and S4†) are presented in the ESI,† and show that these properties are similar to those of polypropylene parts printed by PBF as reported in the literature. The dynamic mechanical properties are discussed in more detail below.

3.5.1. Mechanical performance of parts printed from molecular weight blends. Fig. 8 shows the thermomechanical behavior of the PP printed parts obtained from the DMA. Inspection of Fig. 8 shows that the parts fabricated from the molecular weight blends generally exhibit higher storage and loss moduli than that of the parts fabricated from the pure higher molecular weight PP. For example, at 50 °C, the samples printed from the 12k/250k and 12k/340k powder

Table 1 Molecular weight characteristics of the PP powders prepared *via* the TIPS process

PP samples used in the TIPS process	PP molecular weight of the powders produced *via* the TIPS process		
	M_w/M_n	M_w (1×10^3) Daltons	M_n (1×10^3) Daltons
12k	2.1	17	8.1
250k	2.2	280	130
340k	2.8	360	130
12k/250k (50/50 wt%)	5.8	140	24
12k/340k (50/50 wt%)	6.4	210	33
250k/340k (50/50 wt%)	2.3	300	130
12k/250k/340k (33/33/33 wt%)	14	230	17

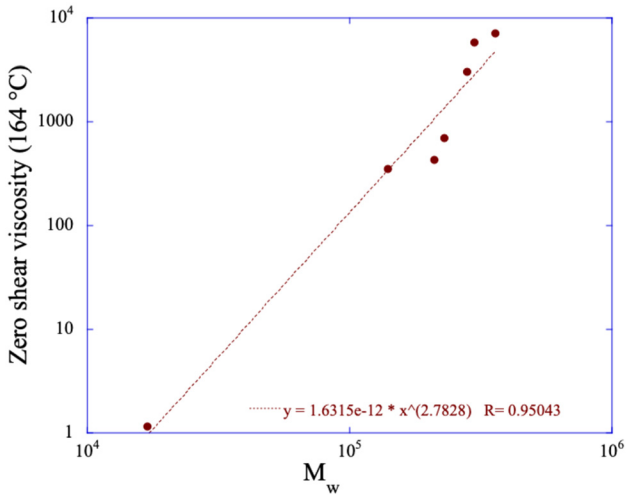

Fig. 6 Zero shear viscosities of PP powders as a function of weight average molecular weight of the polymers.

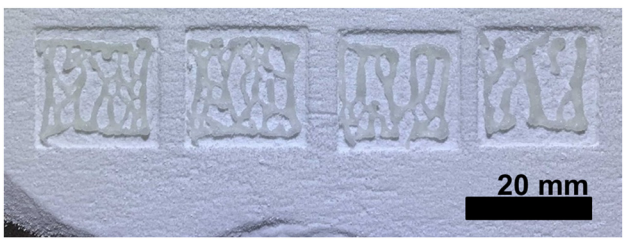

Fig. 7 Single layer scans of the 12k sample resulted in ribbed structures, which did not accurately match the set layer geometry.

exhibit 52% and 194% higher storage modulus than the samples printed from the 250k and 340k powder, respectively. Also, at 50 °C, the addition of 250k to 340k increases the 340k storage modulus of the printed part by approximately 102% and the storage modulus of the part printed from the 12k/250k/340k powder is 15% higher than the storage modulus of the part printed from the 250k/340k powder.

These results are surprising as conventional expectations would suggest that high molecular weight polymers often demonstrate superior mechanical properties compared to their low molecular weight counterparts. Additionally, one might expect that incorporating 12k PP in such large quantities to a high molecular weight polymer would adversely plasticize the polymer system, potentially weakening the mechanical strength of the printed parts. However, the findings presented in Fig. 8 contradict these assumptions. If the 12k additive were indeed causing detrimental plasticization on the polymer matrix, we would expect the mechanical properties of the samples printed from the 12k/250k, 12k/340k, and 12k/250k/340k blend powders to be significantly weaker than those of the samples printed from the 250k, 340k, and 250k/340k blend powders, respectively. Fig. 9 correlates the storage modulus of the printed parts to the polymer dispersity. Fig. S6–S12† present the SEC traces of the polymers and their blend powders. Examination of Fig. 9 quantifies by how much the addition of 12k low molecular weight polypropylene to form molecular weight blends significantly increases the dispersity of the molecular weight blend powders; the data shows that the addition of 12k increases the dispersity of larger polymers by more than 100%. Interestingly, the data in Fig. 9 reveals that the increase in dispersity of the blends by the addition of the 12k polymer results in materials that exhibit superior mechanical properties than the equivalent materials without the 12k PP. This further verifies that the introduction of the 12k PP does not detrimentally plasticize the printed structures. Furthermore, the storage modulus of the printed parts is plotted as a function of their glass transition temperature (T_g) in Fig. 10. Table S2† shows the variation in the T_g values with repeated DMA experiments where available.

Unsurprisingly, the T_g of the polymer increases with increasing molecular weight, as one would expect from free volume theory.[33–35] However, as was observed in Fig. 9, this lowering of T_g does not correspond to a decrease in storage modulus, as might be expected due to plasticization. Rather the samples printed from powders of lower molecular weight are stiffer (*i.e.* higher modulus) than those printed from higher molecular weight powders. This further emphasizes that the addition of 12k PP to larger polymers does not have a detrimental plasticizing effect on the mechanical properties, indicating that the variation in mechanical performance of the various molecular weight blends must be driven by other factors other than plasticization. Hence, the subsequent sections present further analysis and experiments to provide insight into the underlying factors that drive the observed changes in the mechanical properties of the printed samples.

3.5.2. Crystallinity in printed structures and its impact on storage modulus. The addition of lower molecular weight additives to higher molecular weight materials can alter their crystallization processes during the PBF process, influencing changes in the percent crystallinity and crystal structures of the printed part that could contribute to the improved mechanical properties.[36,37] As shown in Fig. 11, the percent crystallinity of the PP printed structures determined by DSC

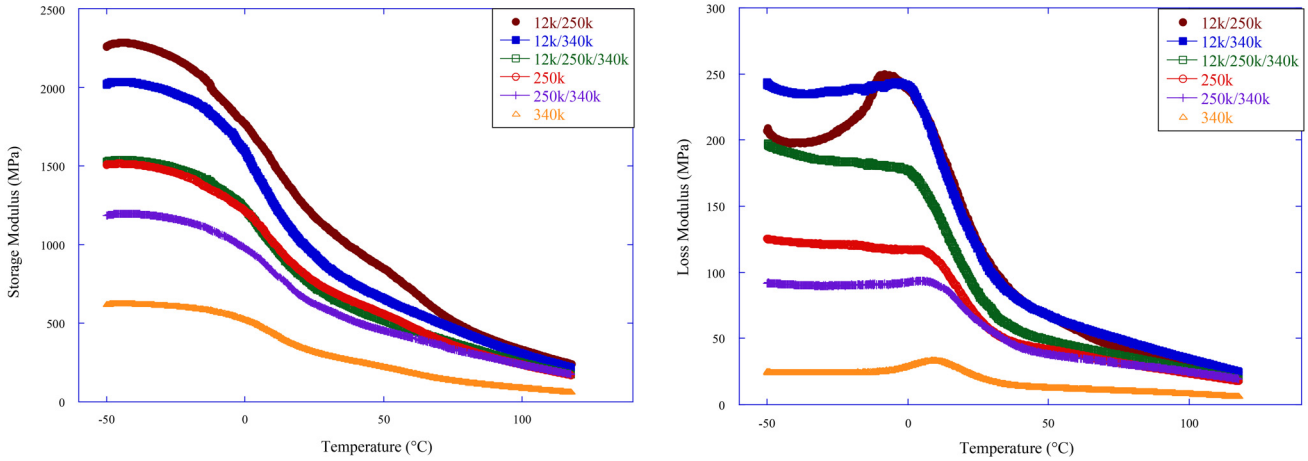

Fig. 8 Thermomechanical properties of the PP printed parts.

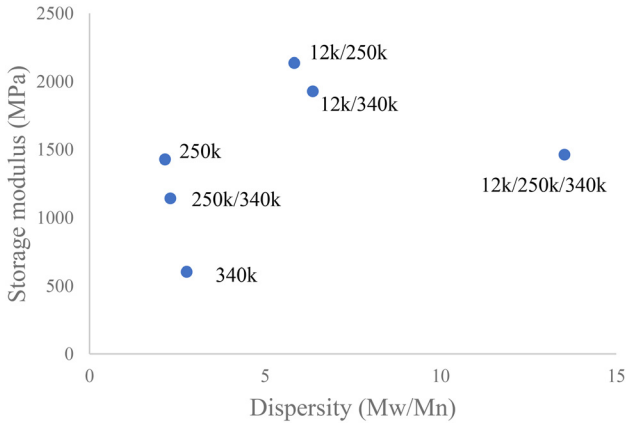

Fig. 9 The storage modulus of the printed parts at −20 °C as a function of the polymer dispersity.

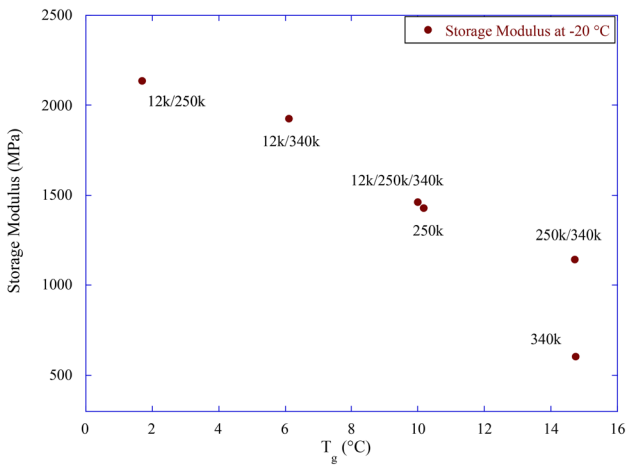

Fig. 10 Storage modulus of the printed structures at −20 °C as a function of T_g.

ranges from 42–50%, which is consistent with previous studies.[36,37]

The addition of 12k PP to the larger polymers resulted in an increase in crystallinity, relative to those that are printed from powders that do not contain 12k PP. Moreover, Fig. 11a shows a strong correlation between percent crystallinity of the printed structure and its storage modulus, where an increase in crystallinity corresponds to a commensurate increase in storage modulus. The dashed box in Fig. 11b shows the storage modulus of melt pressed PP at 50 °C with crystallinities that range from 42–50% as reported by Li *et al.*[37] It is interesting that the moduli of the samples printed from the 12k/250k and 12/340k powders approach the modulus of the melt-pressed PP parts.[37] Comparison of the relationship between % crystallinity and storage modulus of all of the printed samples, however shows that the modulus varies by at least a factor of four when the crystallinity changes from 42 to 50%. This is a much broader range in modulus than the melt-pressed samples, and thus the change in percent crystallinity is not sufficient to account for the observed variation in storage modulus in the printed samples.

Furthermore, the crystal structures of the PP printed parts were examined by WAXS, as under certain conditions, PP can form different crystal structures, including α, β, and γ phases. Studies indicate that the presence of the γ phase in PP significantly contributes to enhancing mechanical performance.[38,39] Moreover, it has been established that lower molecular weight can notably augment the formation of the γ phase in PP,[38,40] and PP can develop various crystalline structures, from spherulites to highly oriented shish-kebabs, which can significantly influence the properties of the printed part.[41]

Fig. 12 shows the wide-angle X-ray scattering of all samples, showing that powder molecular weight does not affect WAXS scattering patterns. The lack of variation in the WAXS patterns indicates that the local ordering of the PP in the crystals is the same for all samples. Thus, the variations observed in the mechanical properties of the printed parts are not attributable

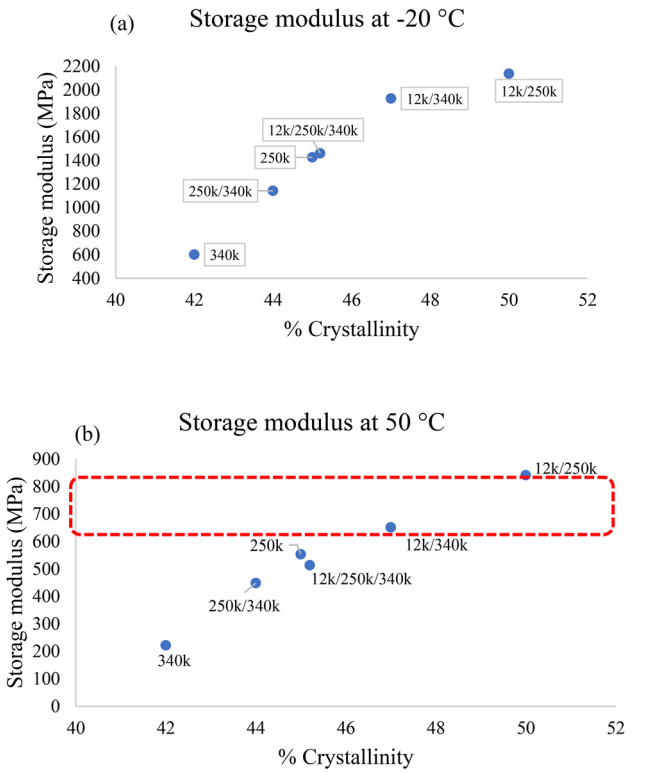

Fig. 11 Correlation of storage modulus with PP crystallinity at −20 °C (a) and 50 °C (b). The dashed box in (b) denotes the modulus of melt pressed PP at 50 °C as reported in Li *et al.*[37]

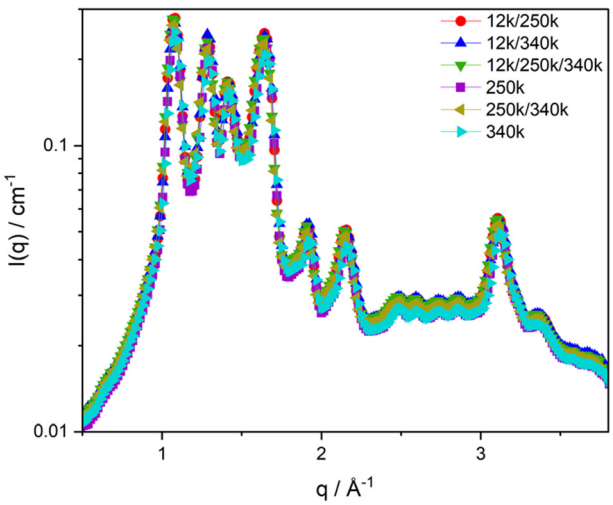

Fig. 12 WAXS scattering patterns of the PP printed parts.

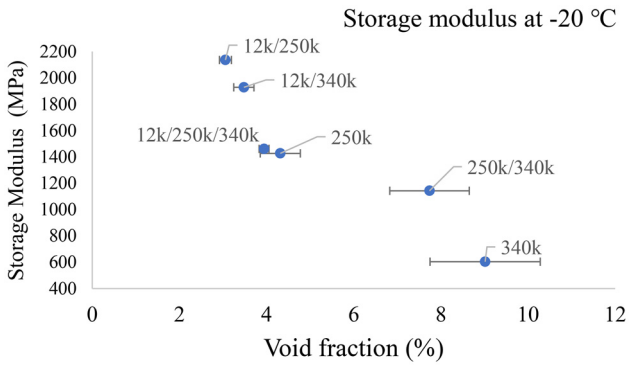

Fig. 13 Storage modulus of the printed PP part at −20 °C as a function of void fraction.

to differences in any change in the packing of the PP molecules in the crystal structures.

3.5.3. Void space in printed structures and its impact on storage modulus. PBF processing often results in parts with microstructural defects, including voids, which can adversely impact the performance of the printed structures. Large voids in PBF parts signify weak interparticle adhesion – often due to incomplete melting and/or incomplete particle coalescence – a detrimental aspect that limits mechanical integrity and consistency in manufactured parts.

The void fraction that is present in each PP printed structure was determined by analyzing SEM images of specimens' freeze-fractures. As shown in Fig. 13, the presence of the 12k PP in the sample appears to decrease the amount of voids in the printed samples. Moreover, there is a strong correlation between the decrease in void space and an increase in storage modulus. This data appears to show that the inclusion of the 12k PP improves the particle coalescence during the printing process, limiting void space in the printed structure. Furthermore, the improved melting and coalescence of the powders results in improved mechanical performance of the printed parts.

We interpret these results to indicate that the incorporation of the low molecular weight 12k PP into the powder increases the molecular mobility of the polymer chain, thus enhancing particle coalescence without varying the print conditions. These results therefore suggest that incorporating a low molecular weight additive in the PBF powder lowers the zero-shear viscosity of the powder, promoting particle coalescence and interparticle adhesion, reducing void space, and thereby strengthening the printed structures.

In fact, the authors' prior droplet coalescence studies quantified how the molecular formulation alters the sintering process,[32] and show that the powders containing 12k PP form substantial neck growth within very short timescales relative to the coalescence of pure molecular weight powders. It is important to emphasize that the exact same batches of powder used in this coalescence study[32] were employed in this printing study to ensure experimental consistency. For instance, the powder formed from the 12k/250k blend achieves 0.8 neck growth in just 4 seconds, while the powder formed from the pure 250k polymer only achieves 0.3 neck growth within the same timeframe.[32] The notable increase in rate of coalescence observed in powders formed from blends with 12k PP additives is attributed to a considerable

reduction in zero shear viscosities, driving enhanced coalescence. Moreover, there is strong agreement between these experimental coalescence studies and the Hopper model, indicating that the 12k PP is homogeneously distributed in the powder and that the improved coalescence is primarily driven by the decrease in zero-shear viscosity.[32] Therefore, these studies demonstrate that molecular formulation of PBF feedstocks can tailor the zero-shear viscosities of powder polymer, enhancing their sintering during the PBF printing process, improving their suitability for the PBF process, and providing a mechanism to augment the overall performance of the structural printed parts fabricated by polymer powder bed fusion.

4. Conclusion

This study describes an innovative approach to tailor the molecular characteristics of polypropylene powder feedstocks for the powder bed fusion (PBF) process *via* thermally induced phase separation (TIPS). Unimodal and molecular weight blend polypropylene powders were fabricated *via* TIPS to examine how their molecular design impacts the PBF process and the properties of the resultant printed part. All powders aside from those formed from 12k PP were printable at the set processing parameters. Failure to print the powder from the 12k PP suggests a minimum zero-shear viscosity to surface tension ratio is necessary to achieve proper coalescence of a scanned layer during the PBF process. Examination of printed parts using these powders shows that the molecular weight blended samples have decreased void space, increased crystallinity, and stronger mechanical properties relative to the parts printed from unimodal powders. Powders fabricated from designed molecular weight blends provide a route to improve the robustness of printed parts by improving coalescence during sintering, reducing void space, and enhanced mechanical properties of the PBF printed parts. These studies thus provide the fundamental understanding of the mechanism by which low molecular weight additives in polymer blends can improve polymer PBF processability and offer pathways to optimize the macroscopic properties of the printed parts. Additionally, the designed protocol in this study can be applied to a variety of materials and processes in PBF additive manufacturing technologies.

Conflicts of interest

There are no conflicts to declare.

Data availability

The data supporting this article have been included as part of the ESI.†

Acknowledgements

Funding for this research was provided by Honeywell Federal Manufacturing and Technologies, LLC.

References

1 C. A. Chatham, T. E. Long and C. B. Williams, A Review of the Process Physics and Material Screening Methods for Polymer Powder Bed Fusion Additive Manufacturing, *Prog. Polym. Sci.*, 2019, **93**, 68–95, DOI: **10.1016/J.PROGPOLYMSCI.2019.03.003**.

2 B. Van Hooreweder, D. Moens, R. Boonen, J. P. Kruth and P. Sas, On the Difference in Material Structure and Fatigue Properties of Nylon Specimens Produced by Injection Molding and Selective Laser Sintering, *Polym. Test.*, 2013, **32**(5), 972–981, DOI: **10.1016/J.POLYMERTESTING.2013.04.014**.

3 C. S. Abbott, M. Sperry and N. B. Crane, Relationships between Porosity and Mechanical Properties of Polyamide 12 Parts Produced Using the Laser Sintering and Multi-Jet Fusion Powder Bed Fusion Processes, *J. Manuf. Process.*, 2021, **70**, 55–66, DOI: **10.1016/J.JMAPRO.2021.08.012**.

4 G. Flodberg, H. Pettersson and L. Yang, Pore Analysis and Mechanical Performance of Selective Laser Sintered Objects, *Addit. Manuf.*, 2018, **24**, 307–315, DOI: **10.1016/J.ADDMA.2018.10.001**.

5 D. L. Bourell, T. J. Watt, D. K. Leigh and B. Fulcher, Performance Limitations in Polymer Laser Sintering, *Phys. Procedia*, 2014, **56**, 147–156, DOI: **10.1016/j.phpro.2014.08.157**.

6 M. Schmid, R. Kleijnen, M. Vetterli and K. Wegener, Influence of the Origin of Polyamide 12 Powder on the Laser Sintering Process and Laser Sintered Parts, *Appl. Sci.*, 2017, 7(5), 462, DOI: **10.3390/app7050462**.

7 D. K. Leigh, A Comparison of Polyamide 11 Mechanical Properties Between Laser Sintering and Traditional Molding, *Int. Solid Freeform Fabr. Symp.*, 2012, 574–605.

8 X. Gong, X. Gao, N. Yu, D. Zhang, L. Tan and J. Li, Characterization of Thermally Treated Polypropylene Powders with Wide Sintering Window for Powder Bed Fusion of Polymers, *Polym. Test.*, 2021, **96**, 107078, DOI: **10.1016/J.POLYMERTESTING.2021.107078**.

9 C. A. Chatham, M. J. Bortner, B. N. Johnson, T. E. Long and C. B. Williams, Predicting Mechanical Property Plateau in Laser Polymer Powder Bed Fusion Additive Manufacturing via the Critical Coalescence Ratio, *Mater. Des.*, 2021, **201**, 109474, DOI: **10.1016/J.MATDES.2021.109474**.

10 F. Lupone, E. Padovano, F. Casamento and C. Badini, in *Materials Process Phenomena and Material Properties in Selective Laser Sintering of Polymers: A Review*, 2021. DOI: **10.3390/ma15010183**.

11 R. D. Goodridge, C. J. Tuck and R. J. M. Hague, Laser Sintering of Polyamides and Other Polymers, *Prog. Mater. Sci.*, 2012, **57**(2), 229–267, DOI: **10.1016/J.PMATSCI.2011.04.001**.

12 B. Wu, K. Zhu, F. Wang, X. Wen, M. Li, Y. Yang and J. Yang, Development of PA6/GO Microspheres with Good Processability for SLS 3D Printing, *Polym. Eng. Sci*, 2022, **62**(5), 1700, DOI: 10.1002/pen.25957.

13 A. Averardi, C. Cola, S. E. Zeltmann and N. Gupta, Effect of Particle Size Distribution on the Packing of Powder Beds: A Critical Discussion Relevant to Additive Manufacturing, *Mater. Today Commun.*, 2020, **24**, 100964, DOI: 10.1016/J.MTCOMM.2020.100964.

14 P. Hejmady, L. C. A. van Breemen, P. D. Anderson and R. M. Cardinaels, Laser sintering of polymer particle pairs studied by in situ visualization, *Soft Matter*, 2019, **15**(6), 1373–1387.

15 S. Dupin, O. Lame, C. Barrès and J. Y. Charmeau, Microstructural Origin of Physical and Mechanical Properties of Polyamide 12 Processed by Laser Sintering, *Eur. Polym. J.*, 2012, **48**(9), 1611–1621, DOI: 10.1016/J.EURPOLYMJ.2012.06.007.

16 S. Berretta, O. Ghita and K. E. Evans, Morphology of Polymeric Powders in Laser Sintering (LS): From Polyamide to New PEEK Powders, *Eur. Polym. J.*, 2014, **59**, 218–229, DOI: 10.1016/j.eurpolymj.2014.08.004.

17 D. Schiochet Nasato and T. Pöschel, Influence of Particle Shape in Additive Manufacturing: Discrete Element Simulations of Polyamide 11 and Polyamide 12, *Addit. Manuf.*, 2020, **36**, 101421, DOI: 10.1016/J.ADDMA.2020.101421.

18 S. Haeri, Y. Wang, O. Ghita and J. Sun, Discrete Element Simulation and Experimental Study of Powder Spreading Process in Additive Manufacturing, *Powder Technol.*, 2017, **306**, 45–54, DOI: 10.1016/J.POWTEC.2016.11.002.

19 X. L. Deng and R. N. Davé, Dynamic Simulation of Particle Packing Influenced by Size, Aspect Ratio and Surface Energy, *Granular Matter*, 2013, **15**(4), 401–415, DOI: 10.1007/S10035-013-0413-0/FIGURES/10.

20 A. V. Gusarov and E. P. Kovalev, Model of Thermal Conductivity in Powder Beds, *Phys. Rev. B:Condens. Matter Mater. Phys.*, 2009, **80**(2), 024202, DOI: 10.1103/PHYSREVB.80.024202.

21 J.-P. Kruth, G. Levy, F. Klocke and T. H. C. Childs, Consolidation phenomena in laser and powder-bed based layered manufacturing, *CIRP Ann. Manuf. Technol.*, 2007, **56**, 730–759.

22 J. Vlachopoulos and D. Strutt, The role of rheology in polymer extrusion, *New Technology for Extrusion Conference*, 2003, 20–21.

23 C. Yan, Y. Shi and L. Hao, Investigation into the Differences in the Selective Laser Sintering between Amorphous and Semi-Crystalline Polymers, *Int. Polym. Process.*, 2011, **26**(4), 416–423, DOI: 10.3139/217.2452/MACHINEREADABLECITATION/RIS.

24 W. Zhu, C. Yan, Y. Shi, S. Wen, C. Han, C. Cai, J. Liu and Y. Shi, Study on the Selective Laser Sintering of a Low-Isotacticity Polypropylene Powder, *Rapid Prototyp. J.*, 2016, **22**(4), 621–629, DOI: 10.1108/RPJ-02-2015-0014/FULL/PDF.

25 N. P. Levenhagen and M. D. Dadmun, Bimodal Molecular Weight Samples Improve the Isotropy of 3D Printed Polymeric Samples, *Polymer*, 2017, **122**, 232–241, DOI: 10.1016/J.POLYMER.2017.06.057.

26 N. Levenhagen and M. D. Dadmun, Improving Interlayer Adhesion in 3D Printing with Surface Segregating Additives: Improving the Isotropy of Acrylonitrile–Butadiene–Styrene Parts, *ACS Appl. Polym. Mater.*, 2019, **1**(4), 876–884, DOI: 10.1021/acsapm.9b00051.

27 K. Guan, Designing Polymer Materials for Improved Additive Manufacturing, Master's Thesis, University of Tennessee, 2021.

28 K. Guan, A. George, M. D. Dadmun, J. S. Bryant, M. J. Bortner and C. B. Williams, Expanding Polymeric Feedstocks for Powder Bed Fusion via Rational Control of Liquid–Liquid Phase Separation, *J. Polym. Sci.*, 2024, **62**(12), 2605, DOI: 10.1002/POL.20230286.

29 Y. Pang, X. Dong, X. Zhang, K. Liu, E. Chen, C. C. Han and D. Wang, Interplay between Crystallization Behaviors and Extensional Deformation of Isotactic Polypropylene and Its Blend with Poly(Ethylene-Co-Octene), *Polymer*, 2008, **49**(10), 2568–2577, DOI: 10.1016/J.POLYMER.2008.03.050.

30 W. W. Yau, A Rheology Theory and Method on Polydispersity and Polymer Long-Chain Branching, *Polymer*, 2007, **48**(8), 2362–2370, DOI: 10.1016/j.polymer.2007.01.073.

31 D. A. Bernard and J. Noolandi, Zero-Shear Viscosity Exponent and Polydispersity Effects, *Macromolecules*, 1982, **15**(6), 1553–1559, DOI: 10.1021/MA00234A018.

32 A. George and M. D. Dadmun, Impact of Polymer Molecular Weight and Dispersity on the Coalescence of Polypropylene Powders Suitable for Laser Powder Bed Fusion, *Polymer*, 2024, **312**, 127663, DOI: 10.1016/j.polymer.2024.127663.

33 K. O'Driscoll and R. Amin Sanayei, Chain-Length Dependence of the Glass Transition Temperature, *Macromolecules*, 1991, **24**(15), 4479–4480, DOI: 10.1021/MA00015A038.

34 S. Askar, L. Li and J. M. Torkelson, Polystyrene-Grafted Silica Nanoparticles: Investigating the Molecular Weight Dependence of Glass Transition and Fragility Behavior, *Macromolecules*, 2017, **50**(4), 1589–1598, DOI: 10.1021/ACS.MACROMOL.7B00079/ASSET/IMAGES/LARGE/MA-2017-000792_0004.JPEG.

35 R. P. White and J. E. G. Lipson, Polymer Free Volume and Its Connection to the Glass Transition, *Macromolecules*, 2016, **49**(11), 3987–4007, DOI: 10.1021/ACS.MACROMOL.6B00215/ASSET/IMAGES/MA-2016-00215G_M024.GIF.

36 J. Arranz-Andrés, B. Peña, R. Benavente, E. Pérez and M. L. Cerrada, Influence of Isotacticity and Molecular Weight on the Properties of Metallocenic Isotactic Polypropylene, *Eur. Polym. J.*, 2007, **43**(6), 2357–2370, DOI: 10.1016/J.EURPOLYMJ.2007.03.034.

37 J. Li, Z. Zhu, T. Li, X. Peng, S. Jiang and L. S. Turng, Quantification of the Young's Modulus for Polypropylene:

Influence of Initial Crystallinity and Service Temperature, *J. Appl. Polym. Sci.*, 2020, **137**(16), 48581, DOI: **10.1002/APP.48581**.

38 W. Zhu, C. Yan, Y. Shi, S. Wen, J. Liu and Y. Shi, Investigation into Mechanical and Microstructural Properties of Polypropylene Manufactured by Selective Laser Sintering in Comparison with Injection Molding Counterparts, *Mater. Des.*, 2015, **82**, 37–45, DOI: **10.1016/j.matdes.2015.05.043**.

39 L. J. Tan, W. Zhu, K. Sagar and K. Zhou, Comparative Study on the Selective Laser Sintering of Polypropylene Homopolymer and Copolymer: Processability, Crystallization Kinetics, Crystal Phases and Mechanical Properties, *Addit. Manuf.*, 2021, **37**, 101610, DOI: **10.1016/j.addma.2020.101610**.

40 D. R. Morrow and B. A. Newman, Crystallization of Low–Molecular–Weight Polypropylene Fractions, *J. Appl. Phys.*, 1968, **39**(11), 4944–4950, DOI: **10.1063/1.1655891**.

41 A. Das, J. S. Bryant, C. B. Williams and M. J. Bortner, Melt-Based Additive Manufacturing of Polyolefins Using Material Extrusion and Powder Bed Fusion, *Polym. Rev.*, 2023, **63**, 895–960, DOI: **10.1080/15583724.2023.2220024**.